

Radiative transfer in decomposed domains

T. Heinemann^{1,2}, W. Dobler^{3,4}, Å. Nordlund², and A. Brandenburg¹

¹ NORDITA, Blegdamsvej 17, DK-2100 Copenhagen Ø, Denmark, e-mail: theine@nordita.dk

² Niels Bohr Institute, Copenhagen University, Juliane Maries Vej 30, DK-2100 Copenhagen Ø, Denmark

³ Department of Physics and Astronomy, University of Calgary, Calgary, Alberta, Canada

⁴ Kiepenheuer-Institut für Sonnenphysik, Schöneckstraße 6, D-79104 Freiburg, Germany

23rd May 2019, Revision: 1.110

Abstract An efficient algorithm for calculating radiative transfer on massively parallel computers using domain decomposition is presented. The integral formulation of the transfer equation is used to divide the problem into a local but compute-intensive part for calculating the intensity and optical depth integrals, and a nonlocal part for communicating the resulting optical depths and radiation intensities between adjacent processor boundaries. The waiting time of idle processors is insignificant because no computations are required during this step. The wall clock time scales nearly linearly with the inverse number of processors. Finally, the method is tested on a realistic simulation of solar convection, and it is found that even in a case with 26 rays the solution of the gray radiative transfer problem takes less than 40 % of the total computing time.

Key words. Radiative transfer - Methods: numerical - Hydrodynamics

1. Introduction

Over the past one or two decades tremendous advances have been made in achieving high resolution power in computational astrophysical fluid dynamics; see Haugen et al. (2003) for a 1024^3 simulation of hydromagnetic turbulence and Kaneda et al. (2003) for a 4096^3 simulation without magnetic fields. Such high resolution is now possible mainly due to the availability of massively parallel computers allowing superb performance at a low price, especially if off-the-shelf personal computers can be interconnected using standard Ethernet switches. This poses no major difficulty for the usual finite difference schemes that allow the computational domain to be decomposed into smaller sub-domains, because the necessary communication between processors is limited to a small neighborhood of the processor boundaries.

Radiative transfer calculations fall generally outside this class of problems, because the transfer equation is intrinsically nonlocal. Physically speaking, information travels at the speed of light when the gas is optically thin. Thus, from one time step to the next, the change in intensity in the domain of one processor can affect the radiation field on many other processors even if they are far apart.

In this paper we describe a simple method that renders the transfer problem essentially local – at least as far as the bulk of the computational cost is concerned. By using the integral formulation of the transfer equation, the intensity may be written as a local integral plus an additive boundary term. The local integral may be computed separately on each processor, whereas the additive term requires successive communication between

neighboring processors. However, this term may be applied after the integrals have been computed on all processors. Thus, contrary to the straightforward calculation, the different processors do not need to wait for this calculation to be completed. Furthermore, after the calculation, all processors have the necessary information to calculate the cooling rates (and, if necessary, the radiative pressure term) at each mesh point and on each processor separately.

This technique has to be contrasted with other popular radiative transfer techniques. Most similar to ours is the multiple wavefront method (Nakamoto et al. 2001). In that case, parallel efficiency is achieved by a special scheme that allows different ray directions to be treated simultaneously, trying to avoid multiple tasks for the same processor and minimizing the number of idle processors. However, our technique appears simpler and remains efficient even for cases where the number of ray directions is small.

We begin by discussing the discretization of the transfer equation and the problems of periodic rays, and then elaborate on the scheme for dividing the problem into local compute-intensive tasks and a nonlocal piece that hardly requires any calculation and hence no waiting.

2. The transfer equation

Radiation couples with the equations of fluid dynamics both through radiative heating and cooling and, if the temperatures are high enough, through radiative pressure. For the applications that we currently have in mind (e.g. stellar convection and

protostellar accretion discs), only heating/cooling is important, so $r \cdot F$ enters the energy equation

$$\frac{D e}{D t} + p r \cdot u + r \cdot F = 0; \quad (1)$$

where ρ is the density, p is the pressure, u is the fluid velocity, e is the internal energy per unit mass, and F measures the energy flux into a fluid element. For radiative energy transfer the energy flux is given by

$$F = \int_0^Z d \cdot d \cdot \hat{r} \cdot I(\hat{r}); \quad (2)$$

where I is the specific intensity giving the amount of energy transported by radiation per unit frequency range per unit area per unit time into a solid angle Ω in the direction \hat{r} .

To determine the specific intensity one has to solve the transfer equation (e.g. Mihalas & Weibel-Mihalas 1984),

$$\hat{r} \cdot r \cdot I = (S - I); \quad (3)$$

where \hat{r} is the unit vector in the direction of propagation, r is the opacity (per unit volume) or inverse mean free path of a photon, and S is the source function, which gives the ratio between emission and absorption.

The transfer equation (3) is here written in its time independent form. This is appropriate for the non-relativistic case, where the maximum fluid velocity is much lower than the speed of light. The flux divergence is then given by

$$r \cdot F = \int_0^Z d \cdot d \cdot (S - I); \quad (4)$$

Following Nordlund (1982), we work with the cooling rate $Q = S - I$ and the optical depth scale $\tau = \int_0^Z ds$, where s is measured along the propagation direction of the ray. It is then possible to rewrite (3) as

$$\frac{dQ}{ds} = \frac{dS}{ds} - Q; \quad (5)$$

This equation may also be written in integral form,

$$Q(\tau) = Q(0)e^0 + \int_0^\tau e^{\tau-s} \frac{dS}{ds} ds; \quad (6)$$

$\boxed{Q^{(\text{intr})}(\tau)}$

where the explicit reference to the frequency τ has been dropped. By using Q instead of I numerical precision is retained even when the optical depth is very high and I approaches S very closely.

In general the source function S may depend on the intensity itself, i.e. on a nonlocal quantity, turning (6) into an integro-differential equation which has to be solved by means of an iterative scheme, such as Accelerated Lambda Iteration (see Olson et al. 1986). In that case the technique outlined here may still be used, but in the following we will restrict ourselves to the case where the source function only depends on local quantities.

Furthermore, we employ a non-staggered Cartesian grid with a set of ray directions chosen in such a way that all rays travel through mesh points, so there is no need for interpolation. As a simple way of implementing boundary conditions, we use ghost zones adjacent to the boundaries.

We stress that the above restrictions have been made solely for the sake of simplicity and are not a prerequisite for the applicability of the parallelization scheme.

3. The radiative transfer scheme

For a source function that only depends on local quantities, the radiative transfer problem, as defined by (5), is in principle easy to solve. Given the cooling rate at a mesh point $n-1$, the discretization of (6) enables us to compute the cooling rate at the next mesh point n in the direction of the ray. Once a given boundary condition is adopted, it is thus possible to determine the cooling rate in the entire simulation box by stepping successively along the ray.

In the case of domain decomposition, only those processors adjacent to a boundary of the simulation box are able to immediately compute the correct cooling rate within their sub-domain. All other processors have to wait until they are provided with boundary information from a neighboring processor that already has determined the correct cooling rate. Without further sophistication, this would imply that most computation related to the radiative transfer problem is not carried out in parallel and valuable CPU time is spent in waiting.

However, for a local source function the integral term $Q^{(\text{intr})}$ in (6) represents a valid solution of the transfer equation within each sub-domain, where the cooling rate vanishes on the boundary. We call this the *intrinsic solution*,

$$Q_n^{(\text{intr})} = Q_{n-1}^{(\text{intr})} e^{-(n-1)\tau} + \int_{n-1}^n e^{-(n-s)\tau} \frac{dS}{ds} ds; \quad (7)$$

with

$$Q_0^{(\text{intr})} = 0 \quad \text{and} \quad \tau_{n-1} = \tau_n - \tau_{n-1}; \quad (8)$$

The complete solution for an arbitrary boundary condition Q_0 may be obtained by simply adding the correction term $Q_0 e^{0-\tau_n}$ to the intrinsic solution at all inner points,

$$Q_n = Q_0 e^{0-\tau_n} + Q_n^{(\text{intr})}; \quad (9)$$

In order to reduce the idle time of the individual processors we thus split the calculation of the cooling rate into three distinct parts, two of which may be carried out by all processors in parallel. How this works out is illustrated in Fig. 1. For the sake of simplicity, the computational domain is two-dimensional and is divided into four equal sub-domains with the same aspect ratio. The transfer equation is solved for rays making a 45° angle with the x axis and pointing to the upper right.

The first step is to obtain the intrinsic solution $Q^{(\text{intr})}$ within each sub-domain, assuming vanishing cooling rate on the boundary. This corresponds to evaluating the integral in Eq. (6). For each point the cooling rate and the optical depth τ are stored. This step can be carried out by all processors

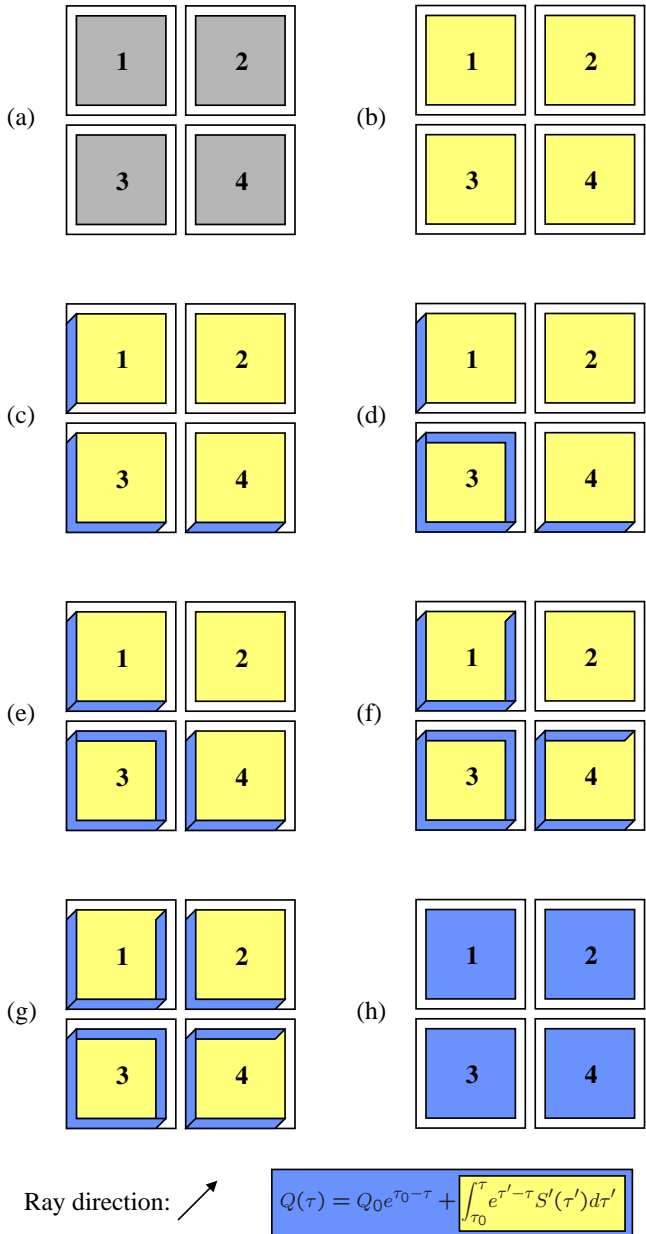


Figure 1. Illustration of the radiative transfer scheme. See text for details.

in parallel since no information is required from outside the processor (Fig. 1b).

The communication part follows next. According to the boundary condition of choice for the entire computational domain, the cooling rate Q_0 is set in the lower ghost zone of processors 3 and 4, as well as in the left ghost zone of processors 1 and 3 (Fig. 1c). Since processor 3 knows the intrinsic optical depth in its sub-domain it can immediately compute the correct cooling rate at its upper and right boundaries by adding the correction term $Q_0 e^{-\tau_0 - \tau_N}$ to the cooling rate obtained from the intrinsic solution. Here τ_0 and τ_N refer to a point in the left (lower) ghost zone and τ_N to the corresponding point at the upper (right) boundary along the ray.

Now that the correct cooling rate at the upper (right) boundary of processor 3 is available, this information is communicated to processor 1 (4) where the boundary condition in the lower (left) ghost zone is set (Fig. 1e). Likewise, processor 1 (4) is now able to compute directly the cooling rate at its right (upper) and can send the values to processor 2 (Fig. 1f and g).

In Fig. 1g all information necessary to solve the full transfer equation at every point on all processors is available and the communication part is finished. The last step is again carried out by all processors in parallel and independently of each other. It amounts to simply adding the correction term $Q_0 e^{-\tau_0 - \tau_N}$, this time to all inner points in the sub-domain (Fig. 1h).

An important aspect of this scheme is that it is actually not limited to the integral solution of the transfer equation as discussed in Sect. 2. The intrinsic solution where an arbitrary but definite boundary condition is employed may equally well be obtained by virtue of any other suitable method. The popular Feautrier method is only one possible choice among several others (Kunasz & Hummer 1974, Mihalas 1974, Auer 1976).

In fact, we have found that on most (but not all) CPUs, the Feautrier method is faster by up to about a factor of two, relative to the most optimized integral method (see the Appendix for details). However, since the integral method is more general (applicable for example also in cases with a combination of Doppler effect and polarization in spectral lines), we choose to present its implementation here.

4. Periodic boundaries

For many applications it is convenient to assume periodicity of the simulation box in one or more spatial dimensions. An example is convection in an infinitely extended plane-parallel layer. While this is trivial to implement for the HD- and MHD-part of a scheme, periodicity introduces a potential difficulty for the radiative transfer scheme.

In the non-periodic case there is always at least one processor where all incoming boundaries are entirely set, once the boundary condition for the whole simulation box has been used. In the example setup of the previous section this would be processor 3. By determining the cooling rate at its outgoing boundaries and communicating to all its neighbors, all incoming boundaries of these neighbors are entirely set, and so on. This implies that each processor has to propagate boundary values only once through its domain.

In contrast to the above, in the case of periodicity it might become necessary to propagate boundary values several times – depending on the ray inclination and the aspect ratio of a processor box – through each sub-domain. This situation is depicted in Fig. 2. The simulation box in this example is divided into two sub-domains along the periodic horizontal direction. As a result of the sub-domains' aspect ratio, each processor has to propagate boundary values twice through its domain. This requires more sophisticated communication than in the non-periodic case but does not pose any fundamental difficulties.

For rays traveling along a periodic direction, there is no boundary condition to start from. However, it is not difficult to see that radiative transfer along periodic rays has a valid and

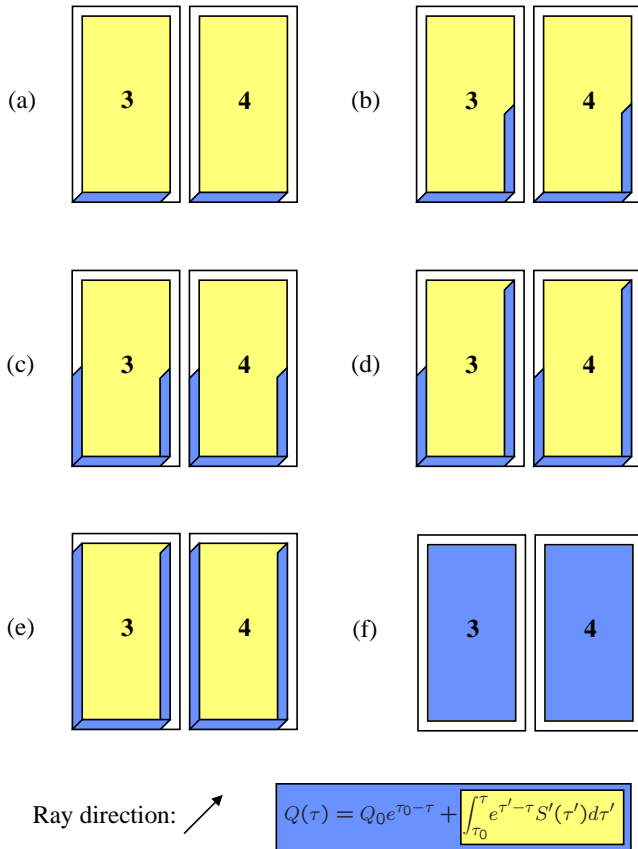


Figure 2. The radiative transfer scheme – Example setup for periodic rays

unique solution. Writing the transfer equation in its integral form,

$$Q_N = Q_0 e^{τ₀ - τ} + \int_{τ₀}^{τ} e^{τ' - τ} \frac{dS}{dτ} dτ ; \quad (10)$$

where the subscripts 0 and N refer to corresponding points on opposite sides of the simulation box, and using the periodicity condition $Q_N = Q_0$, it is possible to solve for the cooling rate Q_0 at the *incoming* boundary,

$$1 - e^{τ₀ - τ} Q_0 = \int_{τ₀}^{τ} e^{τ' - τ} \frac{dS}{dτ} dτ ; \quad (11)$$

In an opaque medium we always have $Q_N > Q_0$.

In a decomposed domain we can obtain the full periodic ray solution in much the same way as in the previous section once Q_0 is known. However, in order to calculate Q_0 itself, communication needs to be done as well, which means that we have to communicate twice through the simulation box.

To minimize waiting times, we use a different communication scheme for periodic rays. Instead of passing the boundary values of the cooling rate successively from one processor to its neighbor, we broadcast the boundary values of the intrinsic cooling rate and the optical depth of each processor simultaneously to all others along the ray. Every processor is then able to calculate Q_0 on its own and no further communication is required.

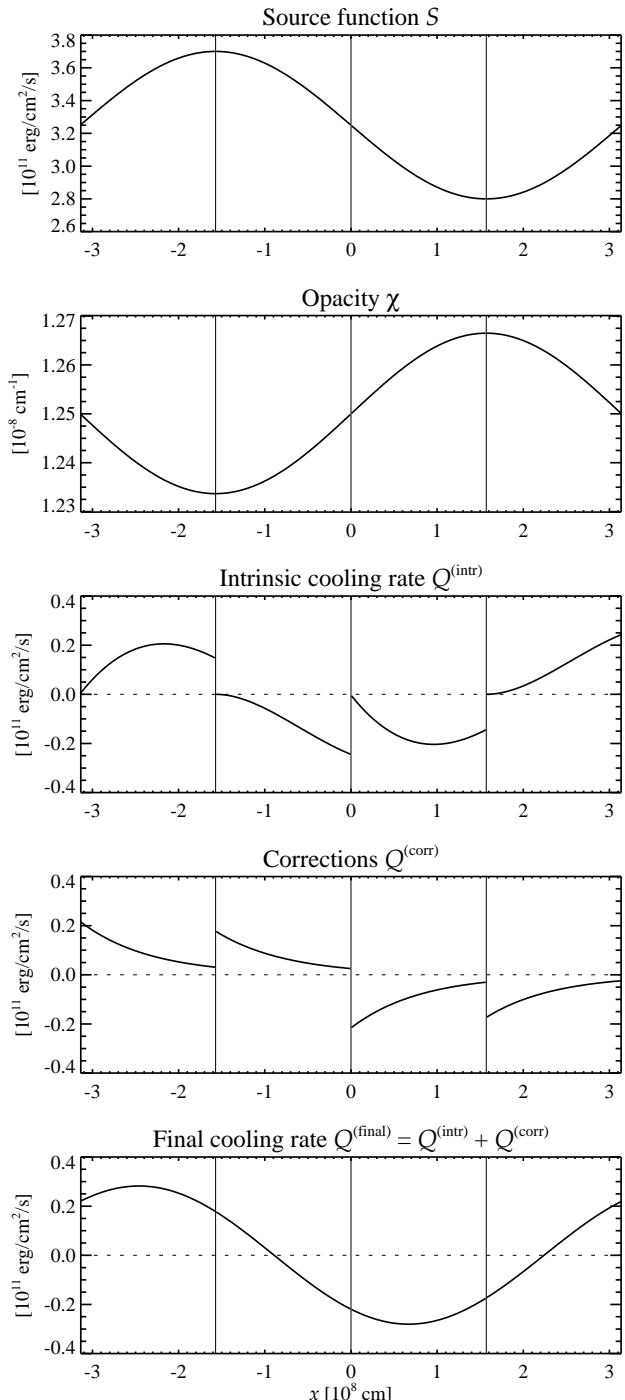


Figure 3. Illustration of the periodic ray solution for one ray traveling in the positive x-direction across 4 processors.

Our measurements show that this communication scheme is indeed more efficient for periodic rays. The reason why we have not implemented it for non-periodic rays is that for inclined rays and sub-domains with arbitrary aspect ratio it becomes rather cumbersome to trace back each ray in order to add up the contributions from those processors the ray has traveled through. However, tracing back the rays is trivial if they travel parallel to a coordinate axis, and for periodic rays in a Cartesian geometry this is always the case.

The periodic ray solution is illustrated in Fig. 3 for a ray traveling in the positive x-direction across 4 processors. The source function and opacity profile are depicted in the two uppermost panels, followed by the intrinsic cooling rate on each processor, the corresponding corrections and the final cooling rate.

5. Implementation and benchmark results

The method for solving radiative transfer problems, as outlined in the previous section, has been implemented into the PENCIL CODE¹. This code has been specifically designed for turbulence simulations in a parallel computing environment using the domain decomposition scheme. The numerical scheme consists of a third order Runge-Kutta method due to Williamson (1980) for the time stepping and sixth order centered finite differences in space; see Brandenburg (2003) for details. The code uses the Message Passing Interface (MPI) for interprocessor communications.

For the numerical solution of the transfer equation we approximate the source function by a second order polynomial in optical depth (see Bruls et al. 1999). The integral in Eq. (6) may then be solved exactly. Numerical details are given in Appendix A.

In order to test the scaling behavior of the parallelization scheme we have performed two benchmark series on the Beowulf cluster at the Danish Center for Scientific Computing. All our tests ran on a subnetwork with 302 Intel Pentium 4 machines with 3.2 GHz CPUs and 1 GB memory. The nodes are connected via Gigabit Ethernet and 10-Gigabit uplinks. On the software side, we used the Intel Fortran Compiler 8.1 and the LAM MPI implementation.

For both benchmark series the number of processors ranges from 1 to 64 in powers of 2, resulting in 7 different calculations. The problem size has been chosen in such a way that there are always 32^3 mesh points in the active region on each processor.

5.1. Radiative MHD benchmarks

In this first benchmark series we compare the scaling performance in ordinary 3-dimensional magnetohydrodynamic (MHD) simulations to those with additional (gray) radiative transfer and therefore partially sequential communication.

The test case is an MHD simulation of the solar surface with the following degrees of sophistication:

1. Plain MHD
2. MHD with hydrogen ionization
3. MHD with hydrogen ionization and radiative transfer

The temperature is obtained iteratively from the entropy using the equation of state, which accounts for hydrogen ionization but ignores the negative hydrogen ion, H^- , and hydrogen molecule formation. The hydrogen ionization fraction and electron number density are obtained as byproducts of the iteration. The H^- opacity is then calculated from the number density of

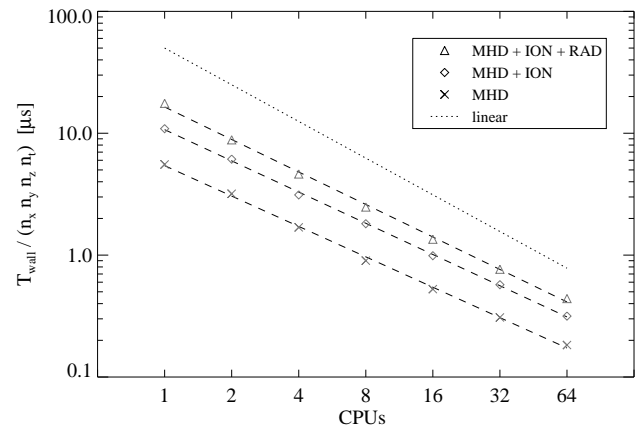


Figure 4. Comparison of the computational expense due to MHD, ionization and radiation for various numbers of CPUs. In the radiation run the transfer equation was solved for 26 ray directions. The wall clock time approximately scales as $n_{\text{CPU}}^{0.82}$, $n_{\text{CPU}}^{0.85}$, and $n_{\text{CPU}}^{0.88}$ for MHD, MHD+ION, and MHD+ION+RAD, respectively. Both here and in Fig. 5 the time is given in terms of wall clock microseconds per mesh point for a full time advance (consisting of three Runge-Kutta sub-steps).

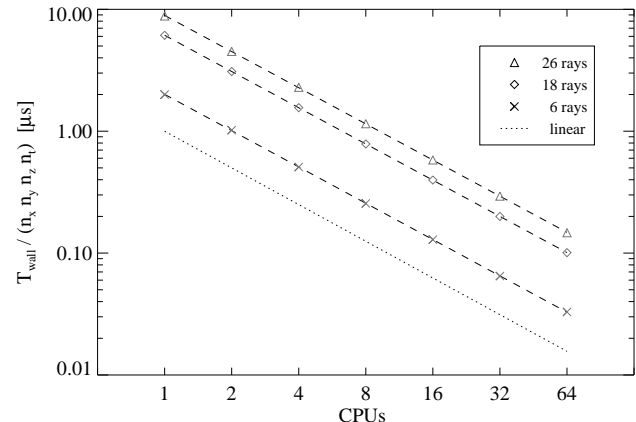


Figure 5. Time consumption for the radiative transfer solver alone using different sets of ray directions. In all three cases the wall clock time scales approximately as $n_{\text{CPU}}^{0.98}$.

H^- , which is again calculated from the number density of electrons and neutral hydrogen. The number density of H^- is very small, so even though H^- is the most important contributor to the opacity, ignoring it in the equation of state is justified.

The timing results from this benchmark series are shown in Fig. 4. The wall clock time scales approximately as $n_{\text{CPU}}^{0.82}$, $n_{\text{CPU}}^{0.85}$ and $n_{\text{CPU}}^{0.88}$ for plain MHD, plain MHD with hydrogen ionization and plain MHD with hydrogen ionization and radiative transfer, respectively. The fact that the scaling exponent approaches 1 as more physics is included indicates that the wall clock time is dominated by the heavier intrinsic calcula-

¹ <http://www.nordita.dk/software/pencil-code>

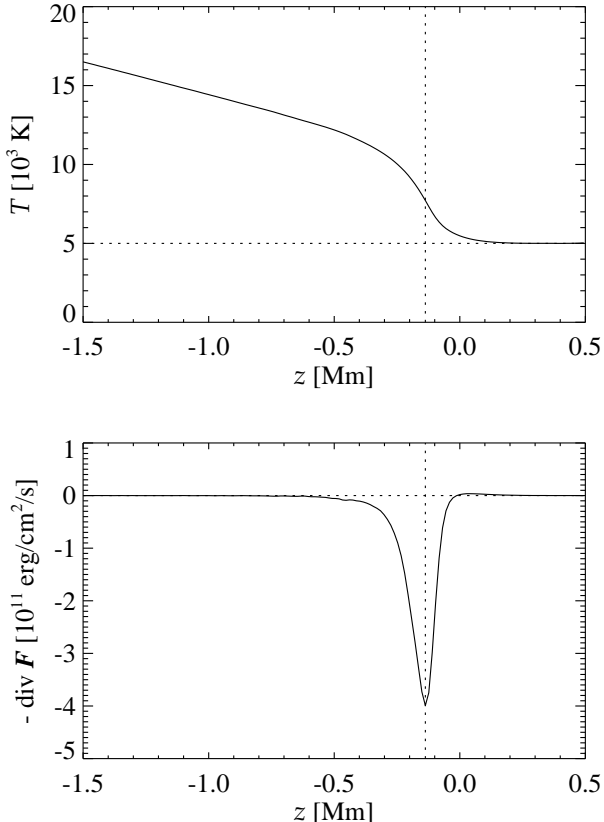


Figure 6. Average temperature as a function of height (top) and average radiative heating as a function of height (bottom). The dashed vertical lines indicate the position of the xy -plane shown in Fig. 7.

tions. Furthermore the sequential nature of the communication process for the radiative transfer solver seems to be insignificant.

5.2. Purely radiative benchmarks

In the second benchmark series we compare the scaling performance of the radiative transfer solver for 3 different sets of ray directions. These sets are determined by the geometry of a grid cell:

1. Rays along the coordinate directions (6 rays)
2. This plus rays along face diagonals (6+12 rays)
3. This plus rays along space diagonals (6+12+8=26 rays)

The test case is the same as in Sect. 5.1.

The reason why we compare the scaling for the above sets of ray directions is that one could expect a decrease in scaling performance as one goes from set 1 to set 3. For rays along the edges of a grid cell there is always a whole layer of processors that can simultaneously receive the boundary cooling rate and propagate it to the next layer. For inclined rays however, the number of processors that can do the communication simultaneously varies as one communicates through the entire domain and is generally less or equal than for rays along the edges.

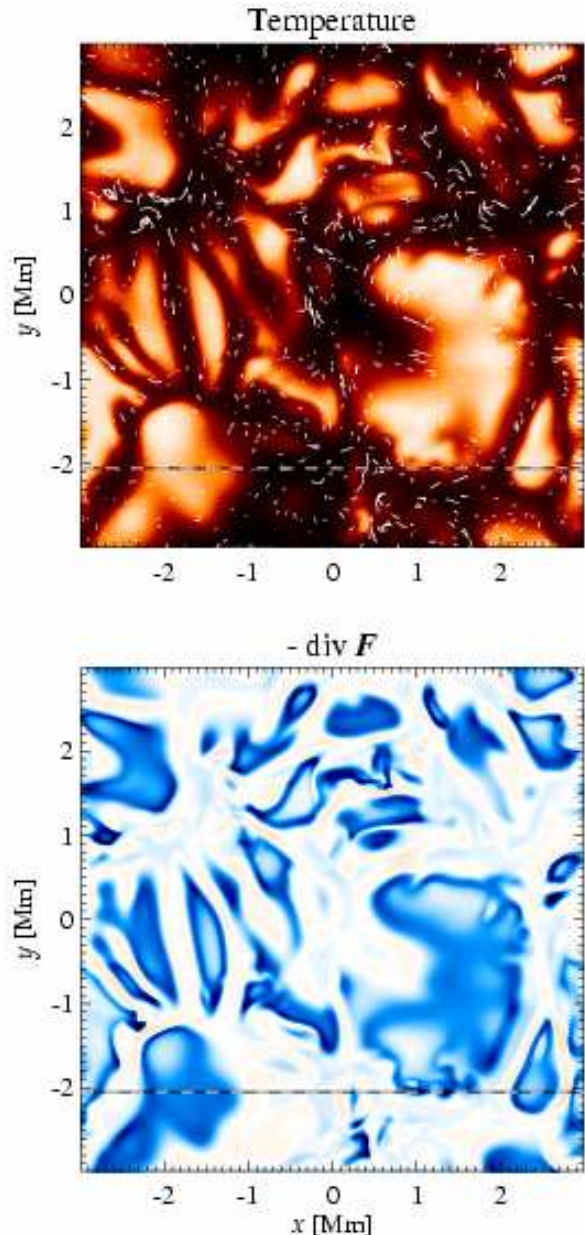


Figure 7. Image of temperature, with magnetic field lines, in a horizontal (xy -) plane near the surface (top). Image of the radiative cooling (blue) and heating (orange) in the same xy -plane (bottom). The dashed lines indicate the position of the xz -plane shown in Fig. 8.

Figure 5 shows the measured wall clock time per mesh point and time step due to radiative transfer for every number of processors and ray direction. The scaling in all 3 cases is almost ideal, i.e. the wall clock time approximately scales as $n_{\text{CPU}}^{0.98}$. This reinforces our previous statement that the partially sequential communication of the radiative transfer scheme has hardly any impact on the scaling.

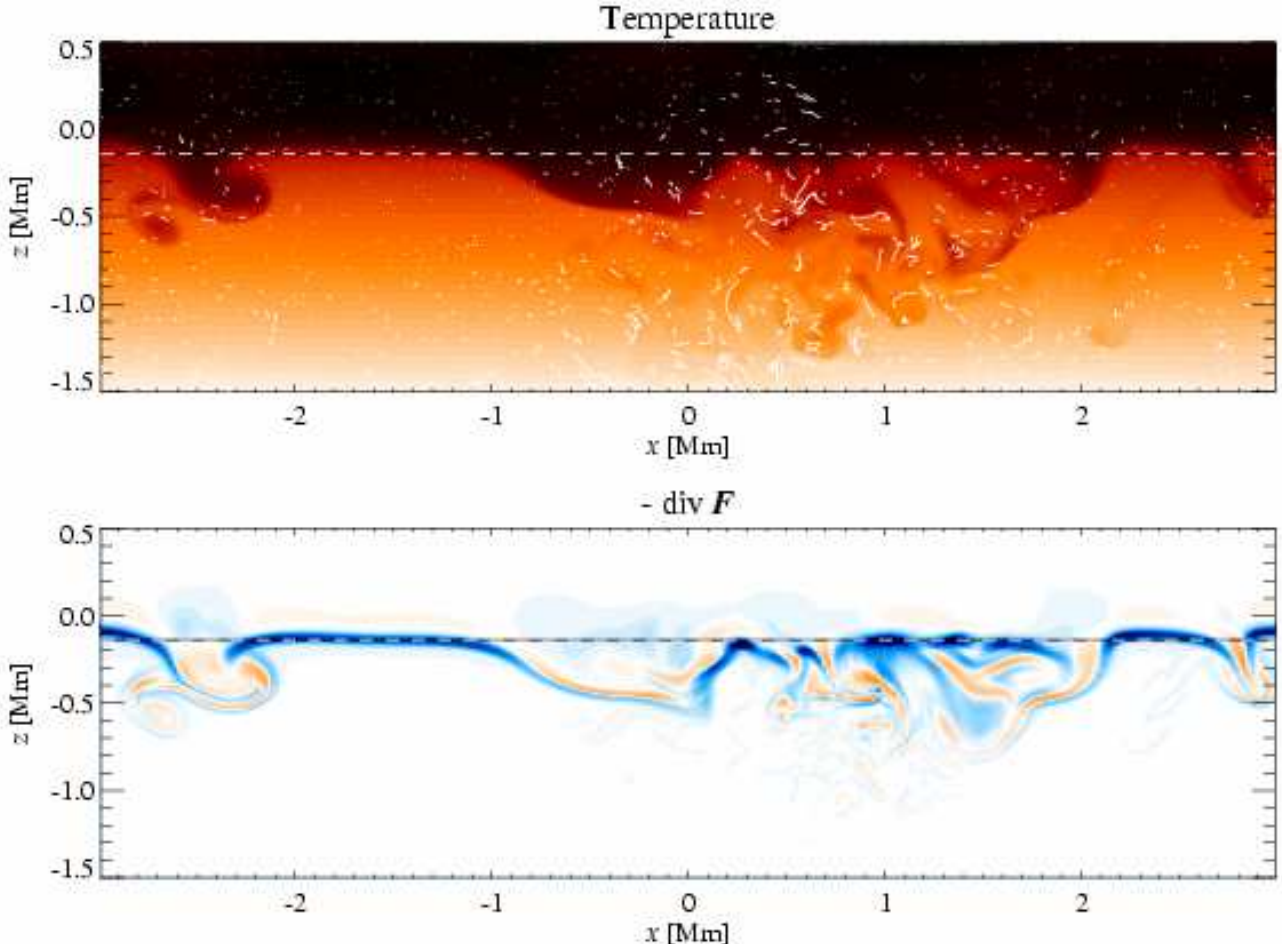


Figure 8. Image of temperature, with magnetic field lines in a vertical (xz-) plane near the surface (top). Image of the radiative cooling (blue) and heating (orange) in the same xz-plane (bottom). The dashed lines indicate the position of the xy-plane shown in Fig. 7.

6. Application to the solar atmosphere

In order to test our radiative transfer scheme under physically meaningful conditions, we now consider a magnetohydrodynamical model of the solar atmosphere near the surface. This requires an accurate treatment of radiative transfer and an equation of state that accounts for hydrogen ionization. Realistic simulations have been carried out by a few groups (Stein & Nordlund 1989, Freytag et al. 1996, Vögler & Schüssler 2003), while in other cases radiation was modeled in terms of the diffusion approximation (e.g. Tao et al. 1998, Cattaneo et al. 2003).

The most important shortcoming of simulations without nonlocal radiative transfer is the lack of a radiative surface. It turns out that this deficit is already cured by using gray radiative transfer along a small number of rays together with a simple opacity law and an equation of state that includes only hydrogen ionization.

The model presented here assumes a gray atmosphere, i.e. the transfer equation is solved in its frequency integrated form. The opacity is taken to be the number density of negative

Hydrogen ions times a fixed absorption cross-section averaged over all frequencies.

All fluid cells are assumed to be in local thermal equilibrium so that the source function S in (5) is given by the Planck function $B = \sigma_B T^4$, which only depends on temperature. This assumption also justifies the determination of the hydrogen ionization degree by virtue of Saha's equation.

The simulation box extends over 6 Mm horizontally and 3.5 Mm vertically. The number of mesh points is 256 \times 256. The transfer equation is solved for rays that travel parallel to the coordinate axes. For a total of 6 rays, the radiative flux divergence is then given by

$$r \cdot F = 4 \int_{\hat{n}_i}^{\hat{x}} Q_i \cdot d\hat{s} \quad (12)$$

The computational box is periodic in the horizontal directions. The initial condition is an isentropic atmosphere in hydrostatic equilibrium with a uniform gravity field of strength appropriate to the solar surface ($g = 275 \text{ m s}^{-2}$). Both fluid velocity and magnetic field are initialized with weak Gaussian noise.

At the top and bottom boundaries the mass density and entropy are antisymmetrically extrapolated around their boundary values, fluid velocity and magnetic vector potential around zero. The cooling rate is assumed to vanish at the bottom boundary ($Q'' = 0$) and to correspond to no incoming intensity at the top boundary ($Q'' = S$).

To prevent numerical instabilities caused by strong shocks reaching the top boundary, the fluid velocity is artificially damped in the uppermost layers. Furthermore, in these layers a relaxation term was added to the energy equation that keeps the temperature close to 5000 K. While the use of these numerical tricks is highly questionable on physical grounds, it allows us to capture the essential features of radiative surface cooling.

Figure 6 shows horizontal averages of temperature and radiative heating after the simulation has run for about 5.5 hours solar time. The surface can be identified with a significant drop in temperature at $z = 0.15 \text{ Mm}$ (indicated by the dashed vertical lines), corresponding to a sharp peak in radiative cooling.

Horizontal slices of temperature and radiative heating at this height are shown in Fig. 7. The gas is cooled most effectively at the edges of the hot convective bubbles, which can be viewed as local surface cooling. The cold gas in between the bubbles tends to be weakly heated.

Figure 8 shows images of temperature and radiative heating in a vertical (xz-) plane (its location is indicated by the dashed lines in Fig. 7). As can be seen, the layer where surface cooling is strong is considerably thinner than the peak shown in Fig. 6, where it was smeared out due to horizontal averaging.

As mentioned above, this simulation also features the evolution of the magnetic field. It is depicted as white arrows in Fig. 7 and Fig. 8. The initial field strength is weak (less than 10^7 gauss), but the field grows due to dynamo action with an e-folding time of about 20 m in. At the time the snapshots were taken the field has not grown enough to have a significant impact on the gas dynamics ($< 10^{22}$). Therefore, in the context of this paper, the inclusion of the magnetic field merely serves as a proof of concept.

7. Conclusions

The present scheme for parallelizing radiative transfer calculations in hydrodynamic simulations in decomposed domains is conceptually simple and straightforward to implement. It is also flexible in the sense that the solution of the transfer equation is not limited to the integral solution but may also be obtained by any other suitable method.

Already in the implementation presented here, one can afford 26 rays per mesh point at a cost of only about 40% of the total time to advance the MHD-equations (including the time to treat ionization in detail, and compute opacities). With the fully optimized integral method, or with the Feautrier method, one can afford 2 to 4 times more rays per point, depending on the CPU and the type of network.

The scheme has proved to work well in a large three-dimensional simulation of the solar atmosphere and is expected to be equally suitable for even larger calculations. As demonstrated in Sect. 5.1, the increased computing load on each processor due to the inclusion of more detailed physics is more

important than the partially sequential communication of the already small amount of data. This means that on up to 64 processors the scaling of the wall clock time with processor number n_{CPU} changes from $n_{\text{CPU}}^{0.82}$ for plain MHD to $n_{\text{CPU}}^{0.88}$ for MHD with ionization and radiative transfer using 26 rays; see Sect. 5.2. The associated increase of CPU time decreases from a factor of 4 on one processor to a factor of about 3 for 64 processors.

We thus conclude that the method is both intrinsically very fast and scales almost linearly with number of CPUs. It is thus ideal in all cases where radiative transfer needs to be included in an accurate manner, with either a large angular resolution alone, or with a large number of angle-frequency points.

The method has been tested successfully for solar convection where even a small number of rays gives already quite useful results (but a more accurate model requires an opacity bin coverage, cf. Stein & Nordlund 1989). After some adjustments of the boundary conditions, the method can also be applied to local simulations of accretion discs using the shearing sheet approximation. Furthermore, by embedding global models of stars or discs into a Cartesian domain, the current implementation of radiative transfer is likely to work even without any further changes; see Freytag et al. (2002) for a similar approach to giant stars.

We have already mentioned several possible ways of extending the scheme, as it is currently implemented in the PENCIL CODE: the inclusion of more rays, a non-uniform vertical mesh, non-gray radiative transfer, radiation pressure, or scattering opacities are all examples of extensions that are still possible within the framework of the parallelization scheme described here.

Appendix A: Numerical details

In order to solve Eq. (6) one has to rely on polynomial approximations for the opacity τ and the source function S , since analytic expressions for these quantities are usually not available. If the opacity is assumed to vary linearly from a particular mesh point n to the next mesh point $n+1$ that lies in the direction of the ray, the difference in optical depth between these points, calculated by the trapezoidal rule, is

$$\tau_{n+1/2} = \frac{1}{2} (\tau_n + \tau_{n+1}) \cdot s_{n+1/2}; \quad (\text{A.1})$$

where $s_{n+1/2}$ is the spatial distance between n and $n+1$. A more accurate (but also more expensive) method is based on a cubic spline fit, using the logarithmic derivative of the opacity,

$$\tau_{n+1/2} = \frac{1}{2} [\tau_n (1 + \frac{1}{6} d_n \cdot s) + \tau_{n+1} (1 - \frac{1}{6} d_{n+1} \cdot s)] \cdot s; \quad (\text{A.2})$$

where

$$d_n = \frac{d \ln \tau}{ds} \Big|_n; \quad (\text{A.3})$$

and, for brevity, we write s instead of $s_{n+1/2}$.

To calculate the heating rate Q''_n due to an ‘upwards’ directed ray, between n and $n+1$ the quadratic Taylor approximation for the source function is used, i.e. we ignore the third and higher derivatives of $S(\cdot)$. Equation (6) then gives

$$Q''_n = a_{n+1/2} Q_{n+1} + b_{n+1/2} S_{n+1}^0 + c_{n+1/2} S_{n+1}^{00}. \quad (\text{A.4})$$

with three coefficients

$$a_{n-1=2} = e^{-n-1=2}; \quad b_{n-1=2} = 1 - e^{-n-1=2}; \quad (A.5)$$

and

$$c_{n-1=2} = e^{-n-1=2} (1 + a_{n-1=2}) - 1; \quad (A.6)$$

similarly, the ‘downwards’ directed rays give

$$Q^{\#} = a_{n+1=2} Q_{n+1} - b_{n+1=2} S_{n+1}^0 + c_{n+1=2} S_{n+1}^{\infty}; \quad (A.7)$$

One observes that in the limit of large optical depth, $(Q'' + Q^{\#})=2$! S^{∞} (diffusion limit). This demonstrates that the second derivative S^{∞} needs to be taken into account, as otherwise the numerically obtained total heating rates will be wrong (they will still be $/ S^{\infty}$ because up- and down-stream contributions do not cancel exactly, but with an incorrect and resolution-dependent coefficient).

We point out that a factor of nearly two in computational speed may be gained in the radiative transfer part of the computations, at the expense of some storage space, by storing and reusing the $e^{-n-1=2}$ factors between two rays in opposite directions. The speed increase was verified in smaller test cases, but the timings presented in Fig. 4 and Fig. 5 were obtained without implementing this.

For small values of τ , the expressions for the coefficients a_n , b_n , and c_n , must be computed in double precision to avoid loss of precision, but the final coefficients may be stored in single precision without noticeable loss of accuracy. On some CPUs further speed-up may be obtained by conditionally using asymptotic expressions for these coefficients, while in other cases, especially where compiler options or special libraries are available to enable vectorization or other optimization of exponentials, it may be faster to retain the explicit computation of exponentials. We have implemented coding that automatically chooses between these two alternatives, based on an initial comparison of the speeds.

The derivatives of S with respect to the optical depth τ have to be computed on an irregularly spaced grid, i.e.

$$S_n^0 = \frac{S_{n-1=2}}{n-1=2} \frac{n+1=2}{2} + \frac{S_{n+1=2}}{n+1=2} \frac{n-1=2}{2} - \frac{\overline{S}_n}{n}; \quad (A.8)$$

$$S_n^{\infty} = \frac{S_{n+1=2}}{n+1=2} - \frac{S_{n-1=2}}{n-1=2} - \frac{\overline{S}_n}{n}; \quad (A.9)$$

where $\overline{S}_n = (S_{n-1=2} + S_{n+1=2})/2$. The procedure to compute radiative energy transport in Cartesian geometry is then straightforward. For each ray direction there are in three dimensions – dependent on the inclination – either one, two or three incoming boundaries where a certain boundary condition is employed and the iteration as defined by (A.4) starts. By moving stepwise through the entire box it is possible to determine the cooling rate at every single mesh point and for all desired ray directions.

Acknowledgements. The work of ÅN was supported by grant number 21-01-0557 from the Danish Research Council for Nature and Universe (FNU). Computing time was provided by the Danish Scientific Computing Center (DCSC).

References

Auer, L. 1976, *J. Quant. Spectr. Rad. Transf.*, 16, 931
 Brandenburg, A. 2003, in *Advances in nonlinear dynamos (The Fluid Mechanics of Astrophysics and Geophysics, Vol. 9)*, ed. A. Ferriz-Mas & M. Núñez (Taylor & Francis, London and New York), 269 [arXiv:astro-ph/0109497]
 Bruls, J. H. M. J., Vollmöller, P., & Schüssler, M. 1999, *A&A*, 348, 233
 Cattaneo, F., Emonet, T., & Weiss, N. 2003, *ApJ*, 588, 1183
 Freytag, B., Ludwig, H.-G., & Steffen, M. 1996, *A&A*, 313, 497
 Freytag, B., Steffen, M., & Dorch, B. 2002, *AN*, 323, 213
 Haugen N. E. L., Brandenburg A., & Dobler W. 2003, *ApJ*, 597, L141
 Kaneda, Y., Ishihara, T., Yokokawa, M., Itakura, K., & Uno, A. 2003, *Phys. Fluids*, 15, L21
 Kunasz, P., Hummer, D. 1974, *MNRAS*, 166, 19
 Mihalas, D. 1974, *ApJS*, 28, 343
 Mihalas, D., & Weibel-Mihalas, B., *Foundations of Radiation Hydrodynamics*, Oxford University Press, 1984
 Nakamoto, T., Umemura, M., & Susa, H. 2001, *MNRAS*, 321, 593
 Nordlund, A. 1982, *A&A*, 107, 1
 Olson, G. L., Auer, L. H., & Buchler, J. R. 1986, *J. Quant. Spectros. Radiat. Transfer*, 35, 431
 Stein, R. F., & Nordlund, Å. 1989, *ApJ*, 342, L95
 Stein, R. F., & Nordlund, Å. 1998, *ApJ*, 499, 914
 Tao, L., Weiss, N. O., Brownjohn, D. P., & Proctor, M. R. E. 1998, *ApJ*, 496, L39
 Vögler, A., & Schüssler, M. 2003, *AN*, 324, 399
 Williamson, J. H. 1980, *J. Comp. Phys.*, 35, 48